Measurement of Time-Varying MIMO Channel for Performance Analysis of Closed-Loop Transmission

Kei Mizutani, Kei Sakaguchi, Jun-ichi Takada, and Kiyomichi Araki
Graduate School of Science and Engineering, Tokyo Institute of Technology
2-12-1 Ookayama, Meguro-ku, Tokyo 152-8550, Japan
Email: kmiz@ap.ide.titech.ac.jp

***Abstract*— A real-time multiple-input multiple-output (MIMO) channel measurement system was implemented by using a 4×4 MIMO software defined radio (SDR) testbed. A target application of this system is to evaluate realistic performance of closed-loop MIMO transmission in time-varying channels at 5GHz band. The results of indoor measurements showed that feedback delay of the closed-loop transmission causes severe degradation of channel capacity, and an interference canceller in eigenbeamspace is indispensable in achieving the benefits of channel state information (CSI) feedback.**

I. Introduction

Multiple-input multiple-output (MIMO) system promises high data rate transmission in rich scattering environments by using multiple antennas both at the transmitter and receiver [1], [2]. In order to exploit its potential capacity, a special condition is assumed: "*perfect* channel state information (CSI) is available at both ends of the transmission channel." For example, space division multiplexing is possible via transmit (Tx) and receive (Rx) beamforming using the CSI, which implies effective utilization of spatial resources to enhance system capacity.

However, the assumption is not realistic especially at the transmitter side. In most cases, CSI estimated at the receiver is fed back to the transmitter for closed-loop transmission, which causes imperfection of the CSI if the channel is not static but temporally varying. Therefore, feedback rate of CSI has to be high enough to track the varying speed of the channel, otherwise, degradation of system performance is inevitable. From the implementation point of view, it is necessary to analyze temporal characteristics of time-varying channels in order to discuss the practical MIMO channel capacity.

Recently, this issue has been studied, e.g. in [3]–[7], by using Jakes' model [8] and Gauss-Markov model [9] to characterize the channel time variation. On the other hand, to the best of our knowledge, analysis based on measured channel data is rare because this kind of data acquisition is not an easy task. Estimated channel data processed in real-time have to be continuously stored which requires sophisticated equipment such as the channel sounders used in [10] and [11].

For the promotion of experimental performance analysis, we developed a real-time MIMO channel measurement system. The measurement system was implemented as an application of our MIMO software defined radio (SDR) testbed [12]. The MIMO-SDR was designed for MIMO extension of 5GHz band orthogonal frequency division multiplexing (OFDM) wireless LAN. An SDR based measurement system has an advantage of hardware and software reusability in contrast with application specific measurement systems. Therefore, results of experiments can be directly linked to system prototyping.

This paper presents indoor measurement results by using the channel measurement system. In order to compare theoretical and realistic performance, channel capacity is calculated with the measured data. We considered three types of closed-loop MIMO transmission models: ideal singular value decomposition (SVD) with perfect knowledge of CSI at the transmitter, feedback SVD with outdated CSI due to feedback delay, and feedback SVD with a zero-forcing (ZF) interference canceller to suppress crosstalk among eigenmodes. Actually, water-filling power allocation is required to maximize theoretical channel capacity, however, it has negative effect if the channel is time-varying [6]. Therefore, we used only Tx weight as CSI to feed back for the closed-loop transmission.

The rest of this paper is organized as follows. System models of the closed-loop MIMO transmission are explained in Section II. Measurement setup, an overview of the measurement system and environment, is described in Section III. In Section IV, the measurement results are presented. Finally, conclusions of this paper are provided in Section V.

In this paper, the following notations will be used. A conjugate, Hermitian transpose and pseudo inverse matrix are denoted by $[\cdot]^*$, $[\cdot]^{\mathrm{H}}$ and $[\cdot]^\dagger$ respectively. $<\cdot>$ indicates the expectation of a random variable. $\mathbf{I}_q$ denotes a $q \times q$ identity matrix. A $q \times q$ diagonal matrix with $a_1, \cdots, a_q$ as its diagonal elements is represented by $\mathrm{diag}(a_1, \cdots, a_q)$.

II. System Model

In this paper, we consider a MIMO-OFDM system with m_{t} Tx and m_{r} Rx antennas. If we focus on a single subcarrier in the frequency domain, the channel can be regarded as narrowband.

The narrowband complex baseband representation of the received signal at time t can be written as

$$\mathbf{r}(t) = \mathbf{H}(t)\mathbf{s}(t) + \mathbf{n}(t), \tag{1}$$

where $\mathbf{r}(t) \in \mathcal{C}^{m_{\mathrm{r}} \times 1}$ is a received signal vector, $\mathbf{s}(t) \in \mathcal{C}^{m_{\mathrm{t}} \times 1}$ is a transmitted signal vector, $\mathbf{H}(t) \in \mathcal{C}^{m_{\mathrm{r}} \times m_{\mathrm{t}}}$ is a channel response matrix and $\mathbf{n}(t) \in \mathcal{C}^{m_{\mathrm{r}} \times 1}$ is a noise vector with zero mean and covariance matrix of $<\mathbf{n}(t)\mathbf{n}^{\mathrm{H}}(t)>= \sigma^2 \mathbf{I}_{m_{\mathrm{r}}}$.

Total Tx power of $\mathbf{s}(t)$ is equally provided to each stream by p as $<\mathbf{s}(t)\mathbf{s}^{\mathrm{H}}(t)>= p\mathbf{I}_{m_{\mathrm{t}}}$. In this paper, the same number of antennas are used both at the transmitter and receiver, i.e. $m_{\mathrm{t}} = m_{\mathrm{r}} = m$.

A. Ideal SVD Model

The MIMO channel $\mathbf{H}(t)$ is estimated at the receiver and SVD is performed as

$$\mathbf{H}(t) = \mathbf{U}(t)\mathbf{D}(t)\mathbf{V}^{\mathrm{H}}(t) \tag{2}$$

to obtain an Rx eigenbeamformer matrix $\mathbf{U}(t) = [\mathbf{u}_1(t), \cdots, \mathbf{u}_m(t)] \in \mathcal{C}^{m\times m}$, a Tx eigenbeamformer matrix $\mathbf{V}(t) = [\mathbf{v}_1(t), \cdots, \mathbf{v}_m(t)] \in \mathcal{C}^{m\times m}$, and a matrix of singular values $\mathbf{D}(t) = \mathrm{diag}(\sqrt{\lambda_1(t)}, \cdots, \sqrt{\lambda_m(t)})$. Here we define the effective channel matrix after eigenbeamforming $\mathbf{H}_{\mathrm{eff}}(t)$ as

$$\mathbf{H}_{\mathrm{eff}}(t) = \mathbf{U}^{\mathrm{H}}(t)\mathbf{H}(t)\mathbf{V}(t). \tag{3}$$

In an ideal SVD model, the received signal vector after eigenbeamforming $\mathbf{y}(t)$ can be modeled as

$$\begin{aligned}\mathbf{y}(t) &= \mathbf{U}^{\mathrm{H}}(t)\{\mathbf{H}(t)\mathbf{V}(t)\mathbf{s}(t) + \mathbf{n}(t)\}\\ &= \mathbf{H}_{\mathrm{eff}}(t)\mathbf{s}(t) + \tilde{\mathbf{n}}(t)\\ &= \mathbf{D}(t)\mathbf{s}(t) + \tilde{\mathbf{n}}(t),\end{aligned} \tag{4}$$

where $\tilde{\mathbf{n}}(t) = \mathbf{U}^{\mathrm{H}}(t)\mathbf{n}(t)$. Since $\mathbf{D}(t)$ is a diagonal matrix and $\mathbf{U}(t)$ is a unitary matrix, this equation denotes that the MIMO channel is decomposed into m parallel SISO subchannels referred to as eigenmodes. SNR of the ith eigenmode at time t is expressed as

$$\gamma_i(t) = \frac{p\lambda_i(t)}{\sigma^2}. \tag{5}$$

Finally, we obtain the channel capacity of the ideal SVD transmission as

$$C(t) = \sum_{i=1}^{m} \log_2\{1 + \gamma_i(t)\}. \tag{6}$$

B. Feedback SVD Model

Here we consider SVD transmission with feedback delay τ which uses a Tx eigenbeamformer matrix $\mathbf{V}(t-\tau)$ at time t. Equations (3) and (4) become

$$\widetilde{\mathbf{H}}_{\mathrm{eff}}(t) = \mathbf{U}^{\mathrm{H}}(t)\mathbf{H}(t)\mathbf{V}(t-\tau) \tag{7}$$

and

$$\begin{aligned}\tilde{\mathbf{y}}(t) &= \mathbf{U}^{\mathrm{H}}(t)\{\mathbf{H}(t)\mathbf{V}(t-\tau)\mathbf{s}(t) + \mathbf{n}(t)\}\\ &= \widetilde{\mathbf{H}}_{\mathrm{eff}}(t)\mathbf{s}(t) + \tilde{\mathbf{n}}(t)\\ &= \mathbf{D}(t)\mathbf{V}^{\mathrm{H}}(t)\mathbf{V}(t-\tau)\mathbf{s}(t) + \tilde{\mathbf{n}}(t).\end{aligned} \tag{8}$$

If $\mathbf{V}^{\mathrm{H}}(t)\mathbf{V}(t-\tau)$ is not an identity matrix, it implies loss of SNR caused by decrease of eigenbeamforming gain and increase of inter-eigenmode interference (IEI). The IEI from the jth eigenmode to the ith eigenmode is written as

$$G_{ij}(t) = |\mathbf{v}_i^{\mathrm{H}}(t)\mathbf{v}_j(t-\tau)|^2, \tag{9}$$

and SNR of the ith eigenmode in this model is expressed as

$$\begin{aligned}\tilde{\gamma}_i(t) &= \frac{p\lambda_i(t)G_{ii}(t)}{\sigma^2 + \sum_{j=1,j\neq i}^{m} p\lambda_i(t)G_{ij}(t)}\\ &= \frac{\gamma_i(t)G_{ii}(t)}{1 + \gamma_i(t)\{1 - G_{ii}(t)\}},\end{aligned} \tag{10}$$

which is a function of two variables, $\gamma_i(t)$ and $G_{ii}(t)$. The channel capacity of this system can be formulated by substituting $\gamma_i(t)$ with $\tilde{\gamma}_i(t)$ in (6).

C. Feedback SVD with ZF Interference Canceller Model

In the model of feedback SVD with a ZF interference canceller, the inverse matrix of (7), $\widetilde{\mathbf{H}}^{\dagger}_{\mathrm{eff}}(t)$, is multiplied to the right hand side of (8) as

$$\begin{aligned}\hat{\mathbf{y}}(t) &= \widetilde{\mathbf{H}}^{\dagger}_{\mathrm{eff}}(t)\{\widetilde{\mathbf{H}}_{\mathrm{eff}}(t)\mathbf{s}(t) + \tilde{\mathbf{n}}(t)\}\\ &= \mathbf{s}(t) + \widetilde{\mathbf{H}}^{\dagger}_{\mathrm{eff}}(t)\tilde{\mathbf{n}}(t).\end{aligned} \tag{11}$$

From (11), the IEI is canceled but noise enhancement is observed due to the multiplication of $\widetilde{\mathbf{H}}^{\dagger}_{\mathrm{eff}}(t)$. SNR of the ith eigenmode in this model is expressed as

$$\hat{\gamma}_i(t) = p\left[\widetilde{\mathbf{H}}^{\dagger}_{\mathrm{eff},i}(t)\{\widetilde{\mathbf{H}}^{\dagger}_{\mathrm{eff},i}(t)\}^{\mathrm{H}}\sigma^2\right]^{-1}, \tag{12}$$

where $\widetilde{\mathbf{H}}^{\dagger}_{\mathrm{eff},i}(t)$ denotes the ith row of $\widetilde{\mathbf{H}}^{\dagger}_{\mathrm{eff}}(t)$ [13]. The channel capacity of this system can be formulated by substituting $\gamma_i(t)$ with $\hat{\gamma}_i(t)$ in (6).

III. Measurement Setup

A. Measurement System

A photograph of the MIMO-SDR is shown in Fig. 1. Six compact PCI boards and a Rubidium (Rb) oscillator are built in a rack. RF components are

- an RF board: four time division duplex (TDD) up/down-converters
- a local oscillator (LO) board: a phase-locked loop (PLL) module.

Reconfigurable baseband components are

- a baseband Tx front-end board: eight digital-to-analog converters (DACs) and five field programmable gate arrays (FPGAs)
- a baseband Rx front-end board: eight analog-to-digital converters (ADCs) and five FPGAs
- a baseband signal processing board: three FPGAs, four digital signal processors (DSPs).

A CPU board is used for user interface and data storage, and the Rb oscillator is the frequency standard of the system. The LO board can provide RF local, IF local and baseband clock signals, however, phase noise of this board is not negligible for channel measurements. Therefore, we used external instruments to provide those signals instead of the LO board. Specifications of the MIMO-SDR are summarized in Table I.

Configuration of the developed measurement system is shown in Fig. 2. A 4-channel baseband signal generator, a 4-channel real-time channel estimator and an RF controller are

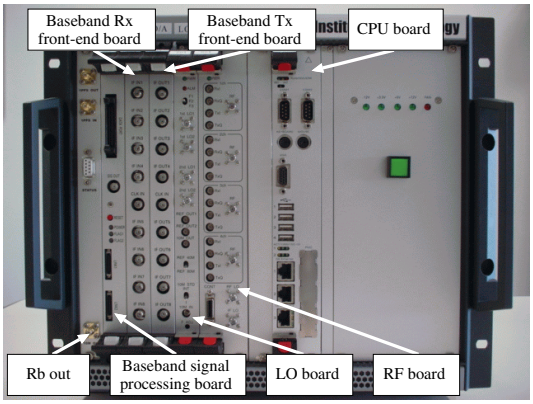

Fig. 1. A photograph of the MIMO-SDR.

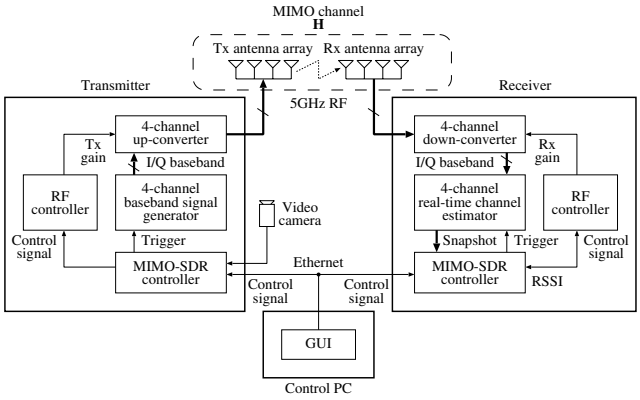

Fig. 2. Configuration of the measurement system.

TABLE I
SPECIFICATIONS OF THE MIMO-SDR.

DAC	14bit, 80MHz × 8 (I/Q × 4)
ADC	14bit, 80MHz × 8 (I/Q × 4)
FPGA	2Mgates × 13
DSP	32bit, 600Mflops × 4
CPU	Pentium M, 1.6GHz
Center frequency	5.04 / 5.06 / 5.08GHz
Bandwidth	20MHz
Tx power	−30 to 10dBm per channel
Frequency stability	10^{-11} (Rb)
RF configuration	Tx × 4 / Rx × 4 (TDD)

implemented in FPGAs on the baseband Tx front-end board, the baseband Rx front-end board and the baseband signal processing board respectively. A MIMO-SDR controller runs on the CPU board, which can be controlled from a remote PC via Ethernet.

At the transmitter, the training signals, modified from the IEEE802.11a [14] preamble to be orthogonal among the Tx channels, are stored in the baseband signal generator and periodically generated every 0.4ms. The I/Q baseband signals are up-converted to 5GHz and transmitted from the 4-element Tx antenna array. At the receiver, the RF signals received by the 4-element Rx antenna array are down-converted to the I/Q baseband signals. Then FFT and channel estimation are processed in FPGAs every 4ms. Finally, the estimated channel responses (snapshots) are continuously loaded by the MIMO-SDR controller and stored in a hard disk. At the same time, the measurement environment is monitored with a video camera from the transmitter side and captured as image data every 100ms.

B. Measurement Environment

The measurements were carried out in a building of Tokyo Institute of Technology at a center frequency of 5.06GHz. An overview of the measurement environment is shown in Fig. 3. The room measures 3.5m by 6m with a height of 2.5m. Conference tables were located in the center of the room and measurement equipment was hidden under the tables. There are two doors to the room and both are made of steel. The Tx and Rx antenna arrays were fixed at a height of 1m for an access point and a user terminal respectively. The array configuration was 4-element uniform linear array with half a wavelength spacing. The Tx and Rx arrays were placed such that broadsides of both arrays were facing each other. Since there was nothing between Tx and Rx antenna arrays, the room was a line of sight (LOS) environment. Although it is reported that fluorescent lights affect the time variation of indoor channels, the effect is relatively small in LOS environments. As a precaution, fluorescent lights in the room were turned off during the measurements. Besides, the measurement environment was monitored with a video camera from the window side.

Three types of scenarios were considered. One was "static" scenario, and the others were "walking" scenarios with different rotations around the tables, "anticlockwise" and "clockwise". In the static scenario, there were no moving objects in the room. On the other hand, in the walking scenarios, a man was walking in the room at a speed of about 1m/s to realize a time-varying propagation channel. Numbers on the walking routes (dashed lines in Fig. 3) indicate the position of the man at time t, which were determined by the captured images as shown in Fig. 4.

IV. MEASUREMENT RESULTS

A. Path Loss

Average path loss of each scenario is calculated as

$$\overline{L(t)} = 10\log_{10}\left\{\frac{1}{m^2 m_{\mathrm{f}}}\sum_{i=1}^{m}\sum_{j=1}^{m}\sum_{k=1}^{m_{\mathrm{f}}}|h_{ijk}(t)|^2\right\}, \qquad (13)$$

where $h_{ijk}(t)$ is the channel response of the kth subcarrier between the jth Tx antenna and the ith Rx antenna, and m_{f} is the number of subcarriers. The results are shown in Fig. 5. The average path loss is flat in the static scenario but fluctuating in the walking scenarios. Degree of fluctuation, i.e. time variation of the channel, depends on the position of the walking man, which was largest when the man passed through the LOS area.

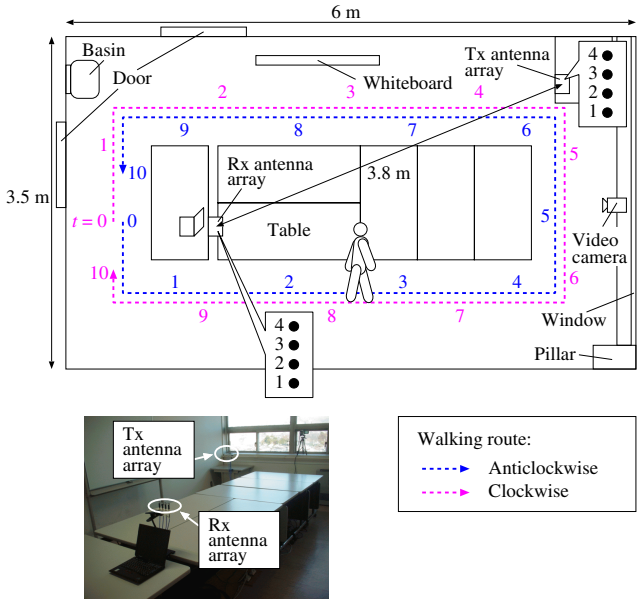

Fig. 3. An overview of the measurement environment.

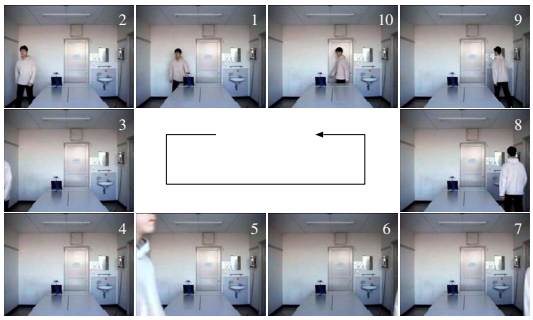

Fig. 4. Captured images in the walking (anticlockwise) scenario.

In the following analysis, we used the data of this worst case in the walking scenarios.

B. Autocorrelation

As a measure of the time variation, autocorrelation $\rho_{ijk}(\tau)$ of the channel responses $h_{ijk}(t)$ at time t and $h_{ijk}(t-\tau)$ at time $t-\tau$ was considered. Here we use discrete time expression as $t = t_0 + nT$ and $\tau = lT$, where t_0 is time of the first snapshot for analysis, n is time index, T is sampling period of snapshots and l is size of time lag. Autocorrelation $\rho_{ijk}(t_0, l)$ within N snapshots was obtained as

$$\rho_{ijk}(t_0,l) = \frac{\sum_{n=0}^{N-1} h_{ijk}(t_0+nT)h^*_{ijk}(t_0+(n-l)T)}{\sqrt{\sum_{n=0}^{N-1}|h_{ijk}(t_0+nT)|^2 \sum_{n=0}^{N-1}|h_{ijk}(t_0+(n-l)T)|^2}}, \quad (14)$$

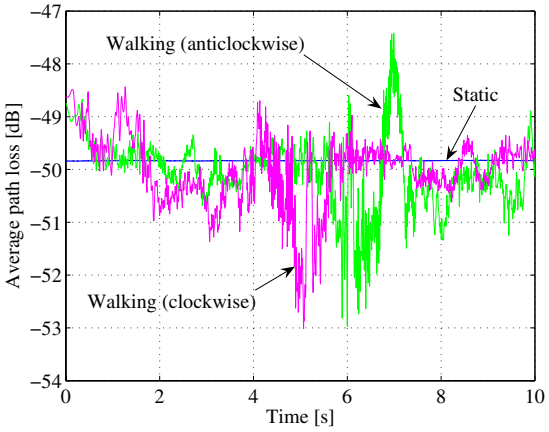

Fig. 5. Average path loss of the snapshots.

and averaged over space and frequency as

$$\overline{|\rho(t_0,l)|} = \frac{1}{m^2 m_{\mathrm{f}}} \sum_{i=1}^{m}\sum_{j=1}^{m}\sum_{k=1}^{m_{\mathrm{f}}} |\rho_{ijk}(t_0,l)|. \quad (15)$$

We chose 500 snapshots (2 seconds) from $t_0 = 5$ for the walking (anticlockwise) scenario and $t_0 = 4$ for the walking (clockwise) scenario, which seem to have similar characteristics with respect to the path loss. In the static scenario, t_0 does not make any difference and we chose $t_0 = 4$. Fig. 6 shows the average autocorrelation with respect to different time lag τ. In the static scenario, the autocorrelation is almost 1, while it falls below 0.9 within 20ms in the walking scenarios.

C. Channel Capacity

Fig. 7 shows the average channel capacity of feedback SVD with a ZF interference canceller ("SVD+ZF"), feedback SVD without interference canceller ("SVD") and ZF without SVD beamforming ("ZF") averaged over m_{f} subcarriers and N snapshots. Although "ZF" is open-loop transmission, it represents the worst case of "SVD+ZF" where SVD beamforming cannot track time variation of the channel and no beamforming gain is obtained. Channel capacity of "ZF" was calculated in the same manner as "SVD+ZF" by using $\mathbf{H}(t)$ instead of $\widetilde{\mathbf{H}}_{\mathrm{eff}}$. Average Rx SNR was set to be 40, 30, 20, and 10dB by normalizing channel responses with average path loss of the snapshots used for the analysis. In the static scenario, the closed-loop transmission remarkably outperform the open-loop transmission, and degradation from the ideal condition (without time lag) is small. This environment can be regarded as static and represents a situation where we can neglect influence of feedback delay. On the other hand, in the walking scenarios, channel capacity of the closed-loop transmission decreases in accordance with the increase in time lag. Especially in "SVD", large degradation can be found in the high SNR cases, and the channel capacity cannot exceed the open-loop transmission if feedback delay is over 12ms, which means that SVD beamforming is a waste of system resource. This critical defect can be improved to some extent by utilizing an

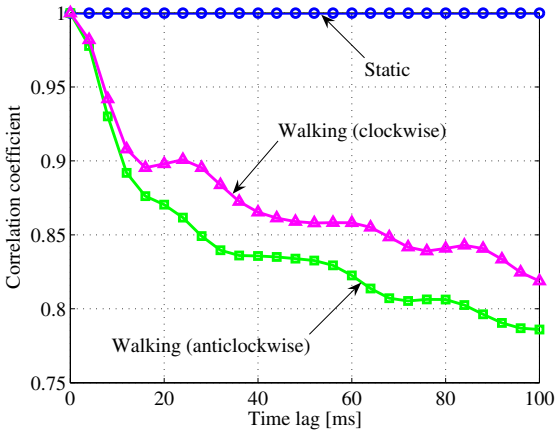

Fig. 6. Average autocorrelation of the channel responses with respect to different time lag.

interference canceller in eigenbeamspace. Therefore, system designers have to keep characteristics of realistic propagation channels in mind in order to optimize system performance.

V. Conclusions

For realistic performance analysis of closed-loop MIMO transmission, we developed a real-time channel measurement system by using a 5GHz band 4×4 MIMO-SDR testbed. The results of the measurements in an indoor environment showed that the time-varying channel considerably degrades channel capacity of the closed-loop MIMO transmission. In order to achieve the benefit of CSI feedback, an interference canceller in eigenbeamspace is indispensable.

In TDD systems, reciprocity of the channel can shorten the updating cycle of CSI, however, calibration of RF circuits is required. For confirmation, we need some modification of the system to measure TDD channels and make it a future work.

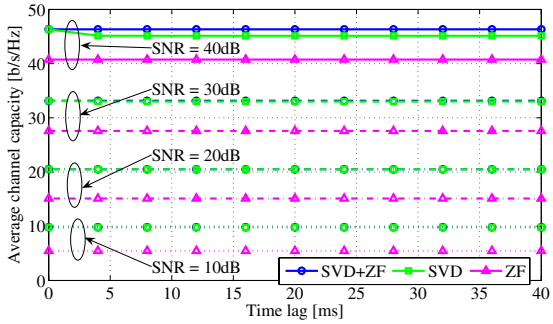

(a) Static scenario.

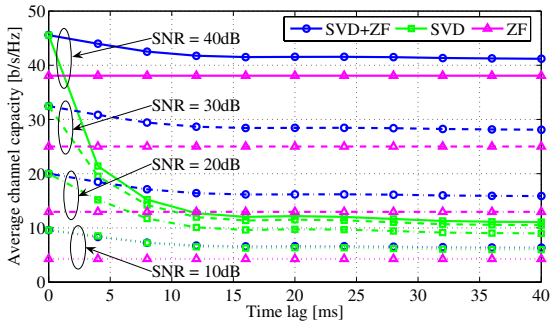

(b) Walking (anticlockwise) scenario.

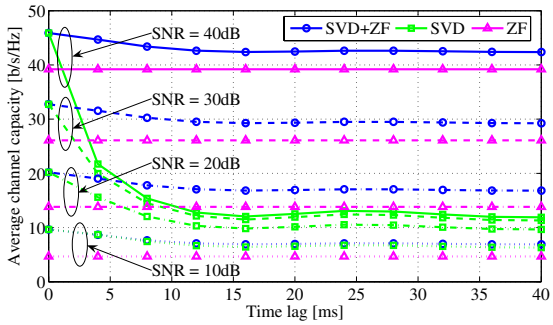

(c) Walking (clockwise) scenario.

Fig. 7. Average channel capacity with respect to different time lag.

References

[1] I. E. Telatar, "Capacity of multiantenna Gaussian channels," *Euro. Trans. Telecommun.*, vol. 10, no. 6, pp. 585–595, Nov./Dec. 1999.

[2] G. J. Foschini and M. J. Gans, "On limits of wireless communications in a fading environments when using multiple antennas," *Wirel. Pers. Commun.*, vol. 6, no. 3, pp. 311–335, Mar. 1998.

[3] S. Ting, K. Sakaguchi, and K. Araki, "Performance analysis of MIMO eigenmode transmission system under realistic channel and system conditions," *IEICE Trans. Commun.*, vol. E87-B, no. 8, pp. 2222–2232, Aug. 2004.

[4] H. T. Nguyen, J. B. Andersen, and G. F. Pedersen, "Capacity and performance of MIMO systems under the impact of feedback delay," in *Proc. IEEE PIMRC 2004*, vol. 1, Barcelona, Spain, Sept. 2004, pp. 53–57.

[5] J. Du, Y. G. Li, D. Gu, A. F. Molisch, and J. Zhang, "Estimation of performance loss due to delay in channel feedback in MIMO systems," in *Proc. IEEE VTC 2004-Fall*, vol. 3, Los Angeles, CA, Sept. 2004, pp. 1619–1622.

[6] G. Lebrun, J. Gao, and M. Faulkner, "MIMO transmission over a time-varying channel using SVD," *IEEE Trans. Wireless Commun.*, vol. 4, no. 2, pp. 757–764, Mar. 2005.

[7] Z. Zhou, B. Vucetic, Z. Chen, and Y. Li, "Design of adaptive modulation in MIMO systems using outdated CSI," in *Proc. IEEE PIMRC 2005*, Berlin, Germany, Sept. 2005.

[8] W. C. Jakes, *Microwave mobile communications*. New York: Wiley, 1974.

[9] S. Haykin, *Adaptive filter theory*, 4th ed. Englewood Cliffs, NJ: Prentice Hall, 2002.

[10] D. P. McNamara, M. A. Beach, and P. N. Fletcher, "Experimental investigation of the temporal variation of MIMO channels," in *Proc. IEEE VTC 2001-Fall*, vol. 2, Atlantic City, NJ, Oct. 2001, pp. 1063–1067.

[11] D. P. McNamara, M. A. Beach, P. N. Fletcher, and P. Karlsson, "Temporal variation of multiple-input multiple-output (MIMO) channels in indoor environments," in *Proc. 11th IEE International Conference on Antennas and Propagation (ICAP 2001)*, vol. 2, Manchester, UK, Apr. 2001, pp. 578–582.

[12] K. Mizutani, K. Sakaguchi, J. Takada, and K. Araki, "Development of 4×4 MIMO-OFDM system and test measurement," in *Proc. 12th European Signal Processing Conference (EUSIPCO 2004)*, Vienna, Austria, Sept. 2004, pp. 689–692.

[13] S. Ting, K. Sakaguchi, and K. Araki, "A robust adaptive MIMO eigenmode transmission system with ZF beamspace interference canceller," in *Proc. IEEE VTC 2005-Spring*, vol. 2, Stockholm, Sweden, May 2005, pp. 859–863.

[14] IEEE, "Wireless LAN medium access control (MAC) and physical layer (PHY) specifications high-speed physical layer in the 5 GHz band," *IEEE Std 802.11a-1999*, 1999.